Characterization of single emitters and nano-antennas

Mohtashami, Abbas

2

Statistical characterization of nitrogen-vacancy centers emission

Nitrogen-vacancy (NV) centers in diamond are generally recognized as highly promising as indefinitely stable highly efficient single-photon sources. We report an experimental quantification of the brightness, radiative decay rate, nonradiative decay rate and quantum efficiency of single NV centers in diamond nanocrystals. Our experiments show that the commonly observed large spread in fluorescence decay rates of NV centers in nanodiamond is inconsistent with the common explanation of large nanophotonic mode-density variations in the ultra-small high-index crystals at near-unity quantum efficiency.

2.1 Introduction

The large promise of quantum-optical technologies to enable secure communication and novel computation architectures sets stringent targets for the quality of photon sources and detectors. In order to meet these demands many efforts are currently devoted to realizing bright sources of single photons [1, 2]. These developments at the same time require novel nanophotonic engineering designs around emitters to enhance light-matter interaction strength as well as indefinitely stable two-level systems that neither bleach, blink, nor spectrally jump. On the nanophotonic engineering side, many different systems have been proposed to control whereto, how fast and with which polarization an emitter emits provided that one manages to locate it exactly

in the right location. These systems include whispering-gallery-mode cavities [2], micropillars and cylindrical wires [3–5], photonic crystal microcavities [6–8], photonic crystal waveguides near cut-off [9, 10], Anderson localizing systems [11], as well as ultrabroadband plasmonic waveguides and antennas [12–15]. Essentially, all these techniques modify the photonic environment of an emitter via the Local Density of Optical States (LDOS) [16, 17]. The LDOS quantifies the light-matter interaction strength that appears in Fermi's Golden Rule for spontaneous emission. Placing the emitter at a position where the LDOS is enhanced, first implies a much higher fluorescence decay rate. Second, if the LDOS enhancement is due to a select set of designed modes as in a cavity or waveguide, the enhanced rate is accompanied by extraction of photons preferentially via these enhanced modes. Thus, photonic engineering promises optimum brightness, dynamics, and collection efficiency. As regards the choice of emitter, a wide variety of systems have been used. Unfortunately, all choices appear to carry large disadvantages when going beyond pilot studies: most dye molecules photobleach [18], II-VI quantum dots [19, 20] blink as well as bleach, and many systems, such as III-V emitters, only have desirable properties when cooled to cryogenic temperatures [3–7, 10, 11]. A promising candidate to provide an indefinitely stable source [21–23] that furthermore allows room-temperature spin-control [24–28] is the nitrogen-vacancy (NV) color center in diamond. NV centers are point defects in diamond structure where a carbon atom is substituted by a nitrogen atom adjacent to a lattice vacancy (figure 2.1(a)). Offsetting their advantageous stability, a disadvantage of NV centers as single photon sources is their very broadband fluorescence emission compared to other quantum-emitters at room temperature, which makes frequency-selective photonic engineering challenging.

When one chooses diamond NV centers as emitters for quantum optics in nanophotonic devices, one can either aim to manipulate emission by fabricating photonic structures directly in diamond [29–31], or one can assemble diamond nanocrystals with photonic structures of a different material [32–39]. Recently, pick-and-place strategies [35–37] were reported in which a single nanoparticle from a diluted powder of diamond nanocrystals dispersed on a substrate is selected and pushed to a desired location by a scanning probe, such as an atomic-force-microscopy tip, or a manipulator in a scanning electron microscope. Reports of this technique span from the coupling of nanodiamonds to photonic-crystal cavities [36, 37] to coupling to plasmonic antennas and nanowires [38, 39]. As a variation of the pick-and-place strategy, a few groups recently developed so called 'scanning-emitter' near-field microscopes in which nanosources are not deposited irreversibly inside a nanostructure, but actually remain attached to a scanning- probe [40–43]. The advantage of such a scanning probe approach is that one can first construct a full map of the LDOS using near-field lifetime imaging to determine where one should ultimately place the nanosource [43]. Microscopy with a light-source as a near-field tip is interesting as a microscopy technique, but only viable if the nanosource is indefinitely stable and does not blink, for which nanodiamonds appear the sole candidate [41, 42, 44–47]. Moreover nanodiamond scanning probes offer the possibility to create nanometer sized local magnetometry probes read out optically by NV spectroscopy [48–51].

In view of the scanning probe microscopy and assembly efforts that seek to combine nanodiamonds and photonic structures, one question stands out as of key importance: given an ensemble of individual nanodiamonds, how does one recognize the ideal nanocrystal? This question is especially relevant given that both fabrication of the photonic structure *and* the intended scanning-probe procedure is highly laborious [35]. Naively, one might think that all nanocrystals of subwavelength size that contain a single NV center will be equally suited, since an NV center is a defect of uniquely defined composition and geometry in the diamond crystalline matrix. However, many workers on diamond nanocrystals have established that NV centers in diamond nanocrystals actually show a distribution of photophysical properties, such as brightness, stability, and decay rates [28, 36, 52–55]. This distribution is usually ascribed to the fact that even though all NV centers are expected to have unit quantum efficiency and the same oscillator strength, these identical unit-quantum-efficiency sources are each differently placed inside their nanoscopic high-index diamond grains [21–23, 53, 55]. This is anticipated to cause different decay rates, due to the fact that the LDOS even in an isolated nanoscopic object varies as a function of position and dipole orientation [56].

In this chapter we address the question how to recognize the ideal nanocrystal from an ensemble of nanocrystals on basis of the requirement that the ideal nanocrystal must contain a single NV center that fluoresces with a high quantum yield, so that it can be useful as a reporting probe of LDOS in nanophotonic systems. We report that the commonly made assumption that NV centers are unit-efficiency dipoles randomly distributed in high index nanoscopic objects is not reconcilable with measured brightness and decay rate histograms data for nanocrystals in the frequently used size ranges around 20–50 nm and 50–150 nm. On basis of the wide distribution of brightness and rate that can not be explained by LDOS variations between nanoparticles alone we conclude that both the radiative and nonradiative rates are broadly distributed.

2.2 Experiment and methods

2.2.1 Sample preparation

Since single NV centers in nanodiamonds are comparatively dim emitters that require high excitation powers, it is essential to avoid background fluorescence when performing fluorescence microscopy. Therefore, we use intrinsically low-fluorescent quartz coverslips (Esco Products) as sample substrates that were cleaned by 15 min sonication in water followed by a 15 min bath in base Piranha (NH_3(aq., 30 %) : H_2O_2(aq., 30 %) : H_2O mixed at ratio 1:1:5, at 75 °C). In our work it is essential that we can unambiguously pinpoint the position of nanodiamonds containing NV centers in the course of the measurement, so that we can revisit the same color center after, for instance, material-deposition steps. To this end we define an array of markers on top of the coverslips using electron-beam lithography. To remove any organic residues after the lift-off process, we treated the coverslips with a mild O_2-plasma descum (Oxford Instruments Plasmalab 80+, using a 5 mTorr,

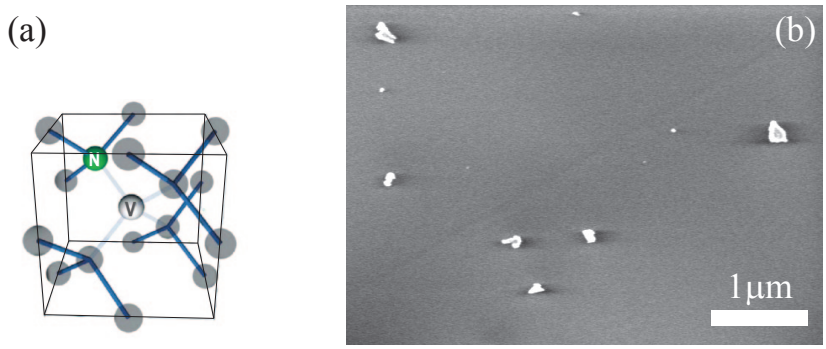

Figure 2.1: (a) Schematic of NV center structure (diagram taken from Ref. [57]). (b) Scanning electron micrograph of dispersed nanodiamonds (Microdiamant MSY 0–0.2) on glass coverslide.

25 sccm O_2 plasma). As sources for NV centers, we use solutions of monocrystalline synthetic nanodiamonds (Microdiamant MSY) with a narrow size tolerance obtained from Microdiamant AG, Lengwil, Switzerland. We note that these nanoparticles have been used recently by a large number of groups in experiments that rely on fluorescence [26, 27, 32, 36, 38, 39, 52–54]. We use these nanodiamonds exactly in the manner as described by Schietinger et al, i.e. without further washing or purification steps [36, 58]. We prepared samples from diamond slurries with two different size distributions by spin-coating aqueous solutions of nanodiamonds that are diluted to a concentration of 1% of the as-received stock solutions on the cleaned and patterned coverslips. The first type of sample, from here on referred to as '25 nm diamond sample' was made from Microdiamant MSY 0–0.05, which nominally has sizes from 0 to 50 nm. These diamonds have a median diameter of 26 nm, with fewer than 1% of the diamonds above 50 nm in size, according to particle sizing performed on this batch of diamonds by the manufacturer. The second type of sample ('100 nm diamond sample') was made from Microdiamant MSY 0–0.2, which nominally has crystal sizes ranging from 0 to 200 nm. This ensemble has crystals with median diameter 108 nm, and fewer than 1% of particles above 175 nm in size, again according to the size-distribution histogram supplied by the manufacturer. Scanning electron microscope (SEM) inspection indicated a size distribution of nanodiamonds consistent with these specifications. The average density of spin-coated nanodiamonds on the coverslips as checked through the SEM images was about 1 to 8 μm^{-2} depending on the sample, assuring that only a few nanodiamonds are illuminated at the diffraction-limited focus of the objective (figure 2.1(b)). Only a small fraction of the nanodiamonds are fluorescent, and an even smaller fraction fluoresces due to an NV center. We identify a diamond as containing at least one NV center, if we can clearly identify the characteristic zero phonon line (ZPL) [21–23, 59] in its emission spectrum according to the criterion we specify in

section 2.2.3. With this criterion, for 100 nm nanodiamonds at an average density of 1 μm^{-2}, we found on average one NV center in an area equal to $50 \times 50\,\mu m^2$, while for 25 nm nanodiamonds at an average density of 5 μm^{-2} we found on average 2 NV centers in a $100 \times 100 \mu\,m^2$ area. These numbers translate to identifying fewer than 0.05% of the 100 nm nanodiamonds, and fewer than 0.001% of the 25 nm diamonds as containing a (single) NV center beyond doubt. Schietinger et al [60] have reported a higher density of NV centers of about 1% for MSY 0–0.05 nanodiamonds. A difference in reported NV center densities could be either due to a different degree of strictness in labeling a fluorescent emitter as an NV center beyond doubt (see section 2.2.3 for our criteria), or alternatively to batch-to-batch variations in nanodiamond slurries.

2.2.2 Experimental setup

The optical setup, sketched in figure 2.2, consists of an inverted confocal fluorescence microscope equipped with a sample scanning piezo stage. NV centers are optically excited at 532 nm using either a frequency-doubled Nd:YAG pulsed laser (Time-Bandwidth, 10 MHz repetition rate) or a continuous-wave (CW) diode laser (CNI). The laser beam is focused through the coverslip to a diffraction-limited spot on top of the sample, using a 100× dry objective with a numerical aperture of 0.9 (Nikon CFI Plan Fluor). The same objective collects the luminescence and guides it through a long-pass filter (580 nm cut-off) before it is imaged on a CCD camera (Nikon DS-Qi1Mc) or confocally detected on one or two avalanche photodiodes (APD) with single-photon sensitivity (both APDs: id Quantique id100-20ULN). The APDs in combination with a sub-nanosecond-resolution 16 channel correlator (Becker & Hickl, DPC-230) allow for single-photon counting. The correlator can perform time-correlated single-photon-counting (TCSPC) lifetime measurements by correlation of detection events with laser pulse arrival times, or photon-photon correlations using multiple APDs. We use a second APD in a Hanbury-Brown and Twiss (HBT) configuration to measure photon correlation statistics (antibunching) at CW excitation. Single-nanocrystal spectra are collected using an imaging spectrometer (SpectraPro 2300i) equipped with a thermoelectrically cooled back-illuminated Si CCD array detector (Princeton Instruments PIXIS:100B).

2.2.3 Measurement procedure to characterize single nanodiamonds

In order to find nanodiamonds containing NV centers, the sample is first pumped with wide-field laser illumination and the fluorescence is imaged on the CCD camera. We use an illumination power of 20 mW, over an area of about 30 μm diameter. Under these conditions, any potential NV center will appear as a diffraction-limited fluorescent spot. Subsequently, we switch to diffraction-limited illumination and position the potential candidate at the laser focus using a piezostage (figure 2.3(a)), and using about 0.5 to 1 mW of power. The fluorescence intensity of the emitter is quantified by integration over a fixed CCD area which is indicated by the green line in figure 2.3(a). At this stage,

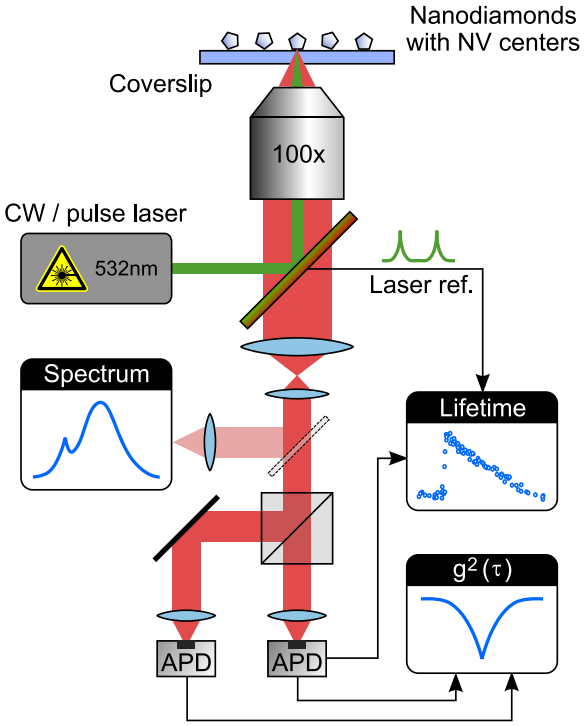

Figure 2.2: Schematic of the experimental setup. Spin-coated nanodiamonds on quartz coverslip are illuminated by 532 nm laser through a 100× dry objective. The emitted fluorescence can be guided to spectrometer or to APDs to measure the lifetime and second order correlation function $g^{(2)}$ of the emitted photons.

we spectrally resolve the fluorescence from the isolated emitter with the spectrometer to specifically find the characteristic zero phonon line of NV centers at a wavelength of about 638 nm (figure 2.3(b)) [21–23]. On basis of the ZPL, we either discard the emitter (absence of ZPL), or identify the nanodiamond as having one or more NV centers (ZPL well above the detector and photon-counting noise). In order to verify that the emission originates from a single center, for each identified NV center, we record a second-order correlation function $g^{(2)}(\tau)$ defined as

$$g^{(2)}(\tau) = \frac{\langle I_1(t) \cdot I_2(t+\tau) \rangle}{\langle I_1(t) \rangle \cdot \langle I_2(t+\tau) \rangle}$$

where $I_1(t)$ and $I_2(t)$ are time-resolved photon counts on each of the two APDs. To this end, we pump the center with the CW laser at a power of about 1 mW to achieve count rates on the order of about 5×10^4 counts per second on each APD and integrate for about 1000 s to obtain reasonable correlation statistics of around 30 coincidences

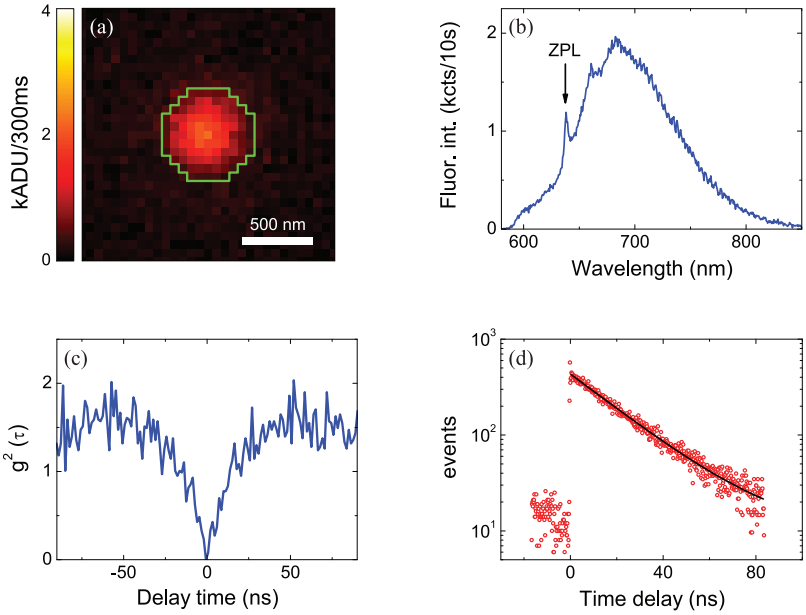

Figure 2.3: (a) CCD image of the fluorescence from a potential NV center positioned at the focus of the laser (1 ADU on our CCD camera corresponds to approximately 6 detected photons). Green line indicates an integration area over which the fluorescence intensity of the emitter is evaluated. (b) Typical spectrum of an NV center expressing the characteristic zero phonon line at 638 nm. (c) Second-order correlation function $g^{(2)}$ of an NV center obtained by CW excitation. The zero dip in $g^{(2)}$ curve confirms the single nature of the center. (d) Background-corrected decay traces of photons emitted from an NV center (red circles, total acquisition time 20 s) with a single-exponential fit (black curve) to extract the lifetime.

per 658 ps bin. Figure 2.3(c) shows a typical background-subtracted $g^{(2)}(\tau)$ curve, with a clearly resolved minimum at zero delay $\tau = 0$ that is well below 0.5, indicating that emission is from a single NV center. Here, the background is subtracted via the procedure reported in [21], based on a measurement directly next to the NV center where we expect identical fluorescence background from the substrate. The background measured only from the substrate shows a Poissonian emission statistics. The bunching in the $g^{(2)}(\tau)$ in figure 2.3(c) at longer delay times (visible at $\tau \approx \pm 50$ ns) is well known to be due to the presence of a shelving state as described by Beveratos et al. [23]. Once we have identified a nanodiamond as containing a single NV center based on its spectrum and antibunching signature, we measure its fluorescence lifetime by switching to pulsed laser excitation. The lifetime of each center is extracted by fitting a single-exponential decay incorporating a small constant background to the decay histogram of emitted photons as shown in figure 2.3(d). We note that the substrate itself has a weak background fluorescence that shows a time dependence. We correct for this artifact by

collecting decay traces from the sample pumped directly next to the NV center. We parameterize the background by a tri-exponential fit (with a dominant sub-nanosecond lifetime) which we subtract from the NV center decay histogram prior to fitting. The residual background is around 10 counts per bin for a total acquisition time of about 20 s.

2.3 Statistics on fluorescence parameters of large nanodiamonds

In this section we report on statistical distributions of the various fluorescence characteristics, i.e. brightness, $g^{(2)}$ and lifetime, that we collected on both nanodiamond size ranges. We first discuss the '100 nm diamond' sample, containing 0–200 nm size nanodiamonds with 108 nm median diameter, and subsequently we discuss the '25 nm diamond' sample with 0–50 nm size nanodiamonds and 26 nm median diameter. For each sample, our statistics is based on identifying 30 to 40 NV centers as described in section 2.2.3.

2.3.1 Distribution of brightness and relation to $g^{(2)}(0)$

As a first step in the characterization process, we have measured the brightness of nanodiamonds that show a clear ZPL line. Figure 2.4(a) shows a histogram of measured brightnesses as quantified by intensity on the CCD at fixed illumination intensity (solid bars). The intensity on the CCD is obtained by summing all pixels within the diffraction-limited image of each diamond (green line in figure 2.3(a)). We observe a wide distribution of intensities, spanning from 50×10^3 to 210×10^3 ADU's (Analog Digital Units) on the CCD per 300 ms exposure time. At an estimated photon-to-ADU conversion factor of 6 for our CCD camera, these brightnesses correspond to 1×10^6 to 4.2×10^6 collected photons per second, at a pump power of 1mW in a diffraction limited spot, supplied by the CW laser. First, these numbers show, at least assuming that NV centers are reasonably efficient emitters, the absorption cross sections of nanodiamond NV centers at 532 nm pump wavelength are an order of magnitude below those of dyes and II-VI quantum dot nanocrystals. Second, there is a wide distribution of brightnesses of over a factor 3 to 4 from nominally identical emitters. As described in section 2.2.3, some nanodiamonds may have multiple NV centers, especially in the case of big nanoparticles. To exclude that brightness variations are due to multiple NV centers, we screen the nanodiamonds on basis of $g^{(2)}$ minimum values. Figure 2.4(b) shows a correlation plot, plotting the fluorescence intensities of all identified NV centers on 100 nm nanodiamond sample versus the recorded value of $g^{(2)}$ at zero delay ($g^{(2)}(\tau = 0)$). We find that not just the brightness, but also the minimum in $g^{(2)}$ is distributed with minima in $g^{(2)}$ ranging from 0 to 0.75. The minimum in $g^{(2)}(0)$ is only weakly correlated with collected intensity, especially via an apparent stepwise increase in the fluorescence intensity as $g^{(2)}(0)$ reaches above ≈ 0.5. Such a stepwise increase would be expected since the minimum in $g^{(2)}$ scales with the number

of emitters n as $1-1/n$. For $g^{(2)}(0) \gtrsim 0.5$ more than a single fluorescent center is involved in the emission, resulting in higher fluorescence intensities on average.

In the remainder we concentrate our analyses on single NV centers, i.e. those nanocrystals for which $g^{(2)}(0) < 0.5$. In figure 2.4(a) , we overplot a histogram of fluorescence intensities of the subset of centers with $g^{(2)}(0) < 0.5$ as patterned bars. The histogram shows a wide fluorescence distribution, with a factor of three difference between brightest and dimmest NV centers, and with a relative distribution of about 30% around the most frequent value. Figure 2.4(b) shows that for the single NV centers the wide distribution in fluorescence intensities notably does not show any correlation to $g^{(2)}(0)$ values.

It should be noted that brightness differences between NV centers could originate from variations in the collection efficiency induced by the different emission dipole moment orientation of each NV center [61]. For the nominal NA of our microscope objective, the detection efficiency for emission of a dipole source is expected to vary as $0.17 + 0.28\sin^2\theta$, as a function of angle θ between dipole and sample surface normal. According to Ref. [62], however, an NV center is not a linear dipole but has two dipole moments of equal size in the plane perpendicular to the NV axis. Our calculations show that for a random distribution of NV orientations, the collection efficiency is centered at around 35%, with 80% of NV centers expected to have collection efficiency between 30% and 40%. Similarly, NV orientation is expected to contribute to a distribution in brightness through orientation-dependent overlap of the absorption dipole with the linear pump polarization. NV orientation hence explains part of, if not the full detected intensity distribution of the NV centers in figure 2.4(a). Further potential causes of brightness variations are variations in the quantum efficiency or the absorption cross-section as well as the dynamics of the metastable state in NV centers [63, 64] that can significantly affect the brightness of an NV center.

2.3.2 Correlation of emission rates and brightness

To examine whether quantum efficiency (QE) effects may be at play, we have measured fluorescence decay rates for each identified single NV center. We plot a histogram of the measured decay rates in figure 2.4(c). We observe a very wide distribution, with the slowest emitters decaying almost 4 times more slowly than the fastest ones. The most frequently occurring decay rate is around $\gamma_{\mathrm{tot}} = 0.03\,\mathrm{ns}^{-1}$ (corresponding to about 33 ns). The time constant of 33 ns is appreciably slower than the fluorescence lifetime of NV centers in bulk diamond, for which the accepted literature value is 11.6 ns [23]. This much slower decay as well as the occurrence of a distribution of rates is in agreement with previously reported values [53, 55]. If the hypothesis that quantum efficiency variations are responsible for the large variability in brightness in figure 2.4(a) is valid, one might expect a correlation between the brightness and decay rate of the emitters. We plot the measured brightness as a function of decay rate for each NV center in figure 2.4(d) which, however, displays no clear correlation. Importantly, we note that the measured quantity here is the total decay rate $\gamma_{\mathrm{tot}} = \gamma_{\mathrm{r}} + \gamma_{\mathrm{nr}}$ which reflects both variations of radiative decay rate γ_{r} and nonradiative decay rate γ_{nr}, whereas

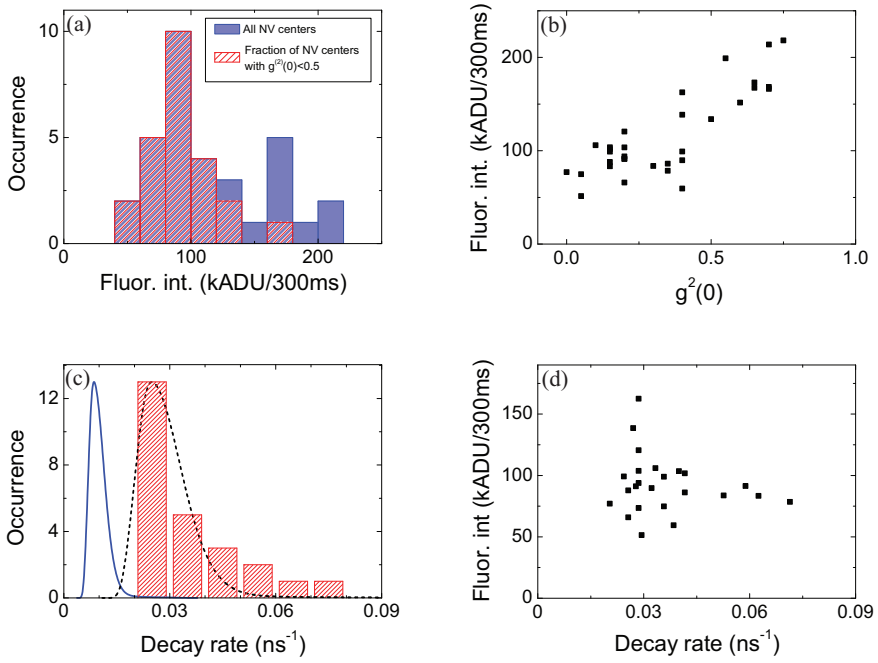

Figure 2.4: Statistics for 100 nm nanodiamonds. (a) Histogram of fluorescence intensity of NV centers (1 ADU on our CCD camera corresponds to approximately 6 detected photons). Solid bars indicate the fluorescence distribution of all identified NV centers whereas patterned bars are related to the fraction of single NV centers identified by $g^{(2)}(0) < 0.5$ in (b). (b) Fluorescence intensity as a function of $g^{(2)}(0)$. (c) Bars: histogram of decay rates of emitters with $g^{(2)}(0)$. Solid line: calculated distribution of LDOS/LDOS$_{vac}$ according to nanodiamond size distribution, normalized to the rate of NV centers in bulk diamond. Dotted line: free scaling of the calculated LDOS distribution (solid line) to match the experimental histogram (bars). (d) Fluorescence intensity as a function of decay rate for emitters with $g^{(2)}(0) < 0.5$ (decay rate error bars are within symbol size). Error bars are comparable to plot symbol size.

the quantum efficiency is given by γ_r/γ_{tot}. Based on the collection efficiency of our microscope (~ 10 %), the count rates in Figure 2.4 correspond to an intermediate (most data) to strong (data point at and above 150 kADU/300 ms))excitation regime, where the photon emission rate is approximately 0.2 to 0.9 times the total decay rate γ_{tot}. Both if one assumes to be in saturation, and below saturation, one expects the fastest decay to imply highest brightness if one assumes γ_{nr} to be approximately constant but γ_r to be distributed. This conclusion is not strongly supported by the data. If conversely we assume γ_r to be approximately constant across NV centers while γ_{nr} is distributed, one would expect highest brightness to correlate with the slowest decay rate (lowest γ_{nr}), a hypothesis also not strongly supported by the data. Specifically, we find that the subset of crystals around the most frequent brightness show the full spread of decay constants, while conversely also the subset of crystals that have decay

constant around the most frequent rate, contain the full range of brightnesses. The lack of strong correlation between decay rate and brightness suggests that the quantum efficiency of NV centers in nanodiamonds as we study here is distributed and not equal to unity for all NV centers. However, as discussed in the previous section, we note that due to variations in the collection efficiency and the unknown dipole orientation of NV centers, the interpretation of brightness in terms of quantum efficiency is convoluted. Therefore, it is essential to use a well-calibrated method in order to determine the quantum efficiency of the NV centers, as we discuss in section 3.3.1.

2.3.3 Common LDOS argument for rate variation in nanodiamond

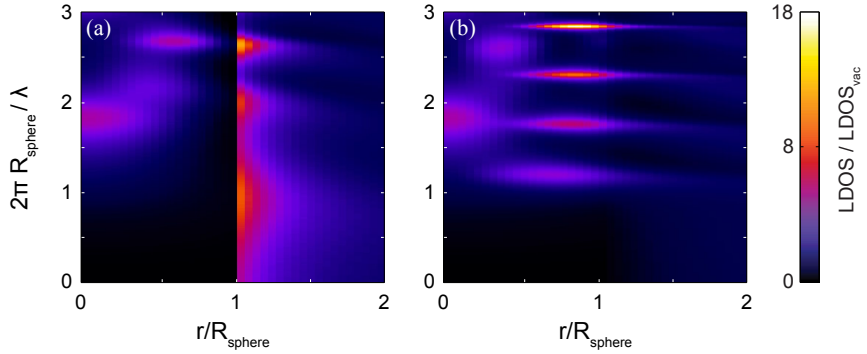

Figure 2.5: LDOS map of dielectric spheres ($\varepsilon_{\text{sphere}} = 5.85$) as function of normalized wavenumber ($2\pi R_{\text{sphere}}/\lambda$) and dipole position in ($r/R_{\text{sphere}} < 1$) and out of ($r/R_{sphere} > 1$) the sphere for (a) radially-oriented, and (b) tangentially-oriented dipole moments. LDOS values are normalized to the value in vacuum.

Many workers had already noticed that nanodiamond decay rates are widely distributed [28, 53, 55]. The variation is commonly attributed to variations solely in the radiative rate γ_{r} due to a local-density-of-photonic-states effect, assuming zero nonradiative decay (i.e. unit quantum efficiency). The hypothesis, explained in detail by Inam et al [53], is that variations are in large part due to the fact that the LDOS experienced by an NV center is influenced by the nanoscale geometry of its environment, i.e. the fact that the source is situated inside, and close to the surface of, a very high index nano-object that is embedded in a low index environment. A distribution in LDOS can arise from the size distribution of nanodiamonds and from the fact that different NV centers have different dipole-moment orientation and positions within the crystals [53, 56]. Here we assess if this LDOS hypothesis is quantitatively reasonable. Considering that the radiative decay rate $\gamma_{\text{r}}(\rho)$ is proportional to LDOS, we evaluate the $\gamma_{\text{r}}(\rho)$ distribution by calculating the LDOS distribution assuming spherical

nanoparticles, for which the LDOS is analytically known [65, 66]. Figure 2.5 shows the calculated LDOS map of diamond spheres as function of normalized wavenumber ($2\pi R_{sphere}/\lambda$) and dipole position in the sphere (r/R_{sphere}) for dipoles oriented normal (a) and tangential (b) to the surface of the sphere. We set the dielectric constant of the spheres equal to the bulk diamond value ($\varepsilon_{\text{sphere}} = 5.85$). For both dipole orientations, LDOS presents a set of resonances with a cut-off at around $2\pi R_{sphere}/\lambda = 1$ inside the sphere. For radially oriented dipoles (figure 2.5(a)), LDOS shows a discontinuity at the boundary of the sphere ($r/R_{sphere} = 1$) which is related to the discontinuity of the out-of-plane component of the electric field at the interface [67]. We modeled nanodiamond NV centers as point dipoles with randomly oriented dipole moments homogeneously distributed in position in the spheres. We furthermore take into account the distribution of particle size as specified according to the nanodiamond size-distribution histogram provided by the manufacturer. We make a histogram of the occurrence of LDOS values to find its probability distribution over all sphere sizes and dipole positions. We take into account the homogenous distribution of all dipole moment orientations by averaging over radial and tangential LDOS values as $\text{LDOS}_{\text{iso}} = \frac{1}{3}\text{LDOS}_{\perp} + \frac{2}{3}\text{LDOS}_{\parallel}$. We fix the wavelength at $\lambda = 680\,\text{nm}$ corresponding to the peak emission wavelength of our NV centers. The resulting LDOS distribution can be converted into a distribution directly comparable to experimentally measured decay rates by scaling the LDOS to the previously reported decay rate of $(11.6\ \text{ns})^{-1} \approx 0.086\,\text{ns}^{-1}$ of NV centers in bulk diamond [23]. We note that this entire procedure involves no adjustable parameter or any fit to data. The final result is plotted in figure 2.4(c) as the solid line. The calculated histogram correctly predicts that emission is significantly decelerated compared to decay in bulk diamond, consistent with the fact that decay in small dielectric spheres is decelerated both compared to vacuum, and bulk dielectric. However, we observe that the calculated histogram peak falls at much lower decay rate than the experimentally measured histogram peak, with a discrepancy amounting to a factor of 3. A similar discrepancy between the calculated and experimentally measured decay rates of nanodiamond NV centers was recently reported for samples with a much wider size distribution, centered at much larger median size, measured by Inam et al [53]. We note that this discrepancy cannot be attributed to the fact that we have taken particle shape to be simply spherical, and that we have neglected the presence of a substrate. These effects cause only small changes in the expected decay rate histogram, as verified in FDTD simulations by Inam et al [53]. One might further argue that the occurrence of a degenerate in-plane dipole moment [62] could skew the histogram of expected decay rates towards higher values, if one assumes the dipole moment is free to diffuse prior to de-excitation. However, if we just make a histogram of the fastest rate instead of the average rate at each possible NV center position, the resulting histogram also does not lead to a consistent explanation (not shown). We conclude that LDOS variations in nanodiamond under the hypothesis of unit quantum efficiency and a bulk decay rate of $(11.6\ \text{ns})^{-1}$ do not explain the variation in measured decay rates.

2.3.4 LDOS argument beyond unit quantum efficiency

Inam et al proposed that although calculated and experimental absolute decay values are inconsistent on basis of LDOS theory and the bulk rate in diamond, the calculated and experimental results can be scaled onto each other. Indeed, if we scale the reference rate that sets the rate axis for the calculated histogram peak not by 11.6 ns (rate constant in bulk diamond [23]), but by a factor of 3 shorter, calculated and measured histogram coincide reasonably (figure 2.4(c) dotted line). Such a scaling would imply as hypothesis a unit quantum efficiency, together with an as yet hidden explanation that introduces a multiplicative correction factor in the calculated rate distribution.

A second hypothesis could be that no adjustment should be made of the bulk rate that enters the comparison, but that the quantum efficiency of NV centers, while unity in bulk, is not unity in nanocrystals. Indeed, an additive offset to the calculated histogram is introduced by nonradiative decay channels that do not occur for bulk diamond, but could occur for nanocrystals due to defects and the presence of large surface area that could contain quenching sites. So far, significant nonradiative decay was evidenced only for very small nanocrystals (5 nm [59]). A distribution of nonradiative rates around $\gamma_{\mathrm{nr}} = 0.15\,\mathrm{ns}^{-1}$ would shift the calculated histogram to the measured rates. The magnitude of the required γ_{nr} implies that quantum efficiencies should be around 30% to 50% for the slowest nanocrystals in the measured ensemble (assuming unit efficiency in bulk).

A third hypothesis could be that the assumption that the bulk rate is entirely radiative to start with, is incorrect, i.e. that the quantum efficiency of NV centers in bulk is significantly below unity contrary to common assumption. Assuming a bulk quantum efficiency of 70% instead of 100% would overlap the calculated histogram peak with the measured most frequent rate. However, this explanation would severely underestimate the width of the decay rate distribution unless a distribution of γ_{nr} is at play.

We conclude that LDOS variations in nanodiamond alone do not explain the variation in measured decay rates, and that a distribution of radiative and nonradiative decay constants must be at play for NV centers in nanodiamond. Furthermore we conclude that an actual experimental calibration of quantum efficiency of individual NV centers is highly desired, which we will return to in sections 3.2 and 3.3.1.

2.4 Statistics on small nanodiamonds

2.4.1 Brightness and $g^{(2)}(0)$

For experiments in which nanodiamonds are intended as probes of, or sources to be embedded in, nanophotonic environments, a size smaller than that of the 100 nm nanodiamonds would be advantageous, as smaller size implies higher spatial resolution and a lower perturbative effect on the modes of the nanophotonic system [68, 69]. Therefore, we repeated the brightness and decay rate statistical measurements for the 25 nm sample, i.e. the batch of crystals with median diameter 26 nm. For 25 nm

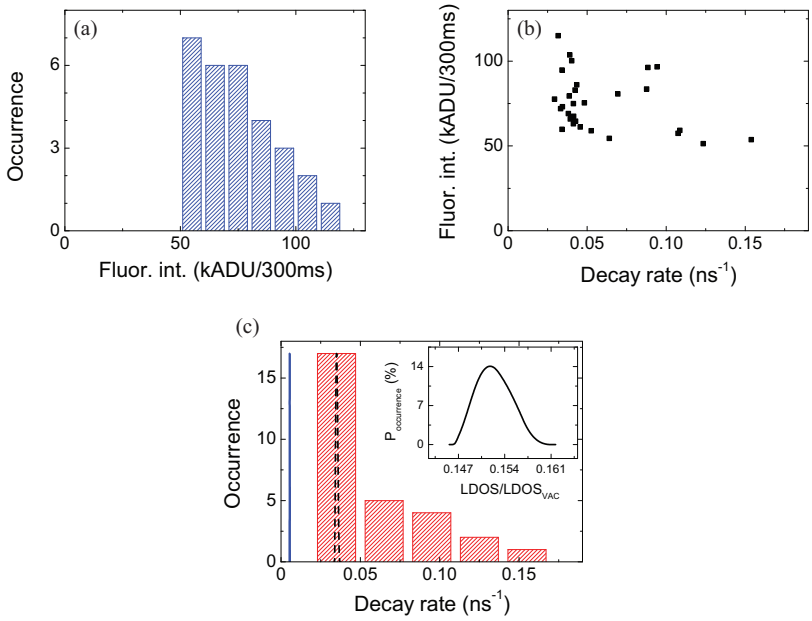

Figure 2.6: Statistics for 25 nm ND. (a) Histogram of fluorescence intensity (1 ADU on our CCD camera corresponds to approximately 6 detected photons). (b) Fluorescence intensity as a function of decay rate. (c) Bars: histogram of the measured decay rates of NV centers. Solid line: calculated distribution of $\mathrm{LDOS}/\mathrm{LDOS}_{vac}$ (shown in the inset) according to nanodiamonds size distribution, normalized to the rate of NV centers in bulk diamond. Dotted line: free scaling of the calculated LDOS distribution (solid line) so to match the experimental histogram (bars).

nanodiamonds, background-subtracted $g^{(2)}$ measurements show a zero dip for all identified NV centers (for a typical 25 nm nanodiamond $g^{(2)}$ see e.g. figure 2.3(c)). The fact that we found no nanodiamonds with multiple NV centers for this sample is commensurate with the smaller average crystal size. For these single NV centers, figure 2.6(a) shows a histogram of the fluorescence intensities measured on the CCD using CW illumination at 1 mW/μm^2. As in the case of the 100 nm sample, the histogram exhibits a wide fluorescence intensity distribution, in this case spanning a factor of about two. The most frequent brightness is approximately a factor two below that of the 100 nm sample.

2.4.2 Distribution of rates

As in the case of the 100 nm nanocrystals, we have also measured the decay rate for all 25 nm nanocrystals that we identified. The decay rate distribution, plotted as a histogram in figure 2.6(c), again shows a very wide distribution, with a factor of 4 contrast in decay rate. We find higher decay rates on average compared to 100 nm

nanodiamonds, with a most frequent decay rate around $\gamma_{tot} = 0.035\,ns^{-1}$ (corresponding to about 28 ns). The most frequent decay rate is approximately 25% faster than for the 100 nm nanodiamonds. Exactly as in the case of 100 nm nanodiamonds, the wide distribution of fluorescence brightness and decay rates does not imply a correlation between the two. As confirmation, in figure 2.6(b) we plot the fluorescence intensities and decay rates of 25 nm diamond NV centers, where we find no clear correlation.

2.4.3 Comparison to LDOS argument for distribution of rates

To assess whether the common hypothesis that the distribution in rate is due to a distribution in LDOS is valid for small nanodiamonds, we calculated the LDOS distribution (plotted in the inset of figure 2.6(c)) also for the 25 nm sample taking into account the size distribution histogram measured by the nanodiamond supplier. The rate distribution expected from the calculated LDOS scaled with the bulk rate (solid line in figure 2.6(c)) is, first, considerably narrower than the experimental decay rate distribution, and second, at considerably reduced rate compared to the measured decay rates. The magnitude of the discrepancy in decay rate is approximately a factor 6, i.e. twice larger than for the 100 nm nanodiamonds. A scaling of the calculated distribution by a multiplicative factor (here a factor of about 6) as proposed by Inam et al [53] does not lead to a good correspondence as in the 100 nm case, as the relative width of the measured histogram far exceeds that of the scaled calculation (dotted line in figure 2.6(c)). Taking our data on both 100 nm and 25 nm nanodiamonds together, we hence do not find support for the hypothesis by Inam et al that a hitherto hidden effect multiplies the radiative rate of NV centers in nanocrystals compared to bulk diamond. A more likely explanation that does not involve a scaling of γ_r due to an unknown origin is that NV centers are subject to a distribution of nonradiative rates on top of the LDOS-induced radiative rate distribution. The measured distribution of 25 nm nanodiamond decay rates points at a wide distribution of nonradiative rates. According to this hypothesis, those crystals with decay around the most-frequent decay rate of $0.035\,ns^{-1}$ must have a quantum efficiency below 15-20%, twice lower than for the 100 nm nanocrystals. The overall lower quantum efficiency estimate is commensurate with the reduction in average brightness, and is also consistent with the fact that a larger sensitivity to nonradiative decay channels is potentially associated with the increased nanocrystal surface-to-volume ratio.

2.5 Conclusions and outlook

In conclusion, we have investigated the brightness and decay rate of single NV centers in nanodiamonds of 25 nm, and of 100 nm median size and studied the brightness and rate distribution and their correlation. For both size ranges a wide distribution in brightnesses and rates is found, consistent with reports by earlier workers. Based on the absence of strong correlation between the measured fluorescence intensity and decay rate of NV centers, we conclude that the quantum efficiency of NV centers

in nanodiamonds is distributed and not equal to unity. In addition, we presented the results of our LDOS-based analytical model for rate distribution of NV centers in nanodiamonds with different sizes. Comparing the analytical results and the measured data, we conclude that the wide distribution of rates is due to a distribution in both radiative and nonradiative rates and therefore the quantum efficiencies of nanodiamond NV centers. This conclusion contradicts earlier work, that interpreted the wide distribution of decay rates as mainly due to a photonic effect that causes a distribution in radiative decay rates via the LDOS.

The fact that the quantum efficiency of nanodiamond NV centers does not correlate with at-hand properties like spectrum or brightness, stands out critically where nanodiamond NV centers are intended to be used as efficient fluorescent sources or LDOS probes in nanophotonic experiments. In other words, screening nanodiamonds to pick the best one to probe LDOS or for incorporation in a photonic device can not rely on a simple metric such as spectrum or brightness. Instead, we argue that future work in the hybrid assembly of nanodiamonds in plasmonics and photonic crystals to realize accelerated spontaneous emission decay always requires an experimental protocol in which nanodiamonds are first individually calibrated in terms of quantum efficiency. Such experimental protocols will be presented in the next chapter where we show, for the first time, the results of quantum efficiency measurements of individual nanodiamond NV centers.

References

[1] C. Santori, D. Fattal, and Y. Yamamoto, *Single-photon devices and applications*, John Wiley & Sons, 2010.

[2] K. Vahala, *Optical microcavities*, volume 5 of *Advanced series in applied physics*, World Scientific, 2004.

[3] J. Bleuse, J. Claudon, M. Creasey, N. S. Malik, J.-M. Gérard, I. Maksymov, J.-P. Hugonin, and P. Lalanne, *Inhibition, enhancement, and control of spontaneous emission in photonic nanowires*, Phys. Rev. Lett. **106**, 103601 (2011).

[4] J.-M. Gerard and B. Gayral, *Strong purcell effect for inas quantum boxes in three-dimensional solid-state microcavities*, J. Lightwave Technol. **17**, 2089 (1999).

[5] J. P. Reithmaier, G. Sek, A. Löffler, C. Hofmann, S. Kuhn, S. Reitzenstein, L. V. Keldysh, V. D. Kulakovskii, T. L. Reinecke, and A. Forchel, *Strong coupling in a single quantum dot-semiconductor microcavity system*, Nature **432**, 197 (2004).

[6] T. Yoshie, A. Scherer, J. Hendrickson, G. Khitrova, H. M. Gibbs, G. Rupper, C. Ell, O. B. Shchekin, and D. G. Deppe, *Vacuum Rabi splitting with a single quantum dot in a photonic crystal nanocavity*, Nature **432**, 200 (2004).

[7] D. Englund, D. Fattal, E. Waks, G. Solomon, B. Zhang, T. Nakaoka, Y. Arakawa, Y. Yamamoto, and J. Vučković, *Controlling the spontaneous emission rate of single quantum dots in a two-dimensional photonic crystal*, Phys. Rev. Lett. **95**, 013904 (2005).

[8] S. Noda, M. Fujita, and T. Asano, *Spontaneous-emission control by photonic crystals and nanocavities*, Nature Photon. **1**, 449 (2007).

[9] P. Yao, V. Manga Rao, and S. Hughes, *On-chip single photon sources using planar photonic crystals and single quantum dots*, Laser & Photon. Rev. **4**, 499 (2010).

[10] H. Thyrrestrup, L. Sapienza, and P. Lodahl, *Extraction of the β-factor for single quantum dots coupled to a photonic crystal waveguide*, Appl. Phys. Lett. **96**, 231106 (2010).

[11] L. Sapienza, H. Thyrrestrup, S. Stobbe, P. D. Garcia, S. Smolka, and P. Lodahl, *Cavity quantum electrodynamics with anderson-localized modes*, Science **327**, 1352 (2010).

[12] A. V. Akimov, A. Mukherjee, C. L. Yu, D. E. Chang, A. S. Zibrov, P. R. Hemmer, H. Park, and M. D. Lukin, *Generation of single optical plasmons in metallic nanowires coupled to quantum dots*, Nature **450**, 402 (2007).

[13] R.-M. Ma, R. F. Oulton, V. J. Sorger, G. Bartal, and X. Zhang, *Room-temperature sub-diffraction-limited plasmon laser by total internal reflection*, Nat. Mater. **10**, 110 (2011).

[14] A. F. Koenderink, *Plasmon nanoparticle array waveguides for single photon and single plasmon sources*, Nano Lett. **9**, 4228 (2009).

[15] A. G. Curto, G. Volpe, T. H. Taminiau, M. P. Kreuzer, R. Quidant, and van Hulst, Niek F, *Unidirectional emission of a quantum dot coupled to a nanoantenna*, Science **329**, 930 (2010).

[16] R. Sprik, B. A. van Tiggelen, and A. Lagendijk, *Optical emission in periodic dielectrics*, Europhys. Lett. **35**, 265 (1996).

[17] L. Novotny and B. Hecht, *Principles of nano-optics*, Cambridge University Press, 2006.

[18] B. Lounis and M. Orrit, *Single-photon sources*, Rep. Prog. Phys. **68**, 1129 (2005).

[19] C. A. Leatherdale, W.-K. Woo, F. V. Mikulec, and M. G. Bawendi, *On the absorption cross section of CdSe nanocrystal quantum dots*, J. Phys. Chem. B **106**, 7619 (2002).

[20] C. de Mello Donegá, S. G. Hickey, S. F. Wuister, D. Vanmaekelbergh, and A. Meijerink, *Single-step synthesis to control the photoluminescence quantum yield and size dispersion of CdSe nanocrystals*, J. Phys. Chem. B **107**, 489 (2003).

[21] R. Brouri, A. Beveratos, J.-P. Poizat, and P. Grangier, *Photon antibunching in the fluorescence of individual color centers in diamond*, Opt. Lett. **25**, 1294 (2000).

[22] C. Kurtsiefer, S. Mayer, P. Zarda, and H. Weinfurter, *Stable solid-state source of single photons*, Phys. Rev. Lett. **85**, 290 (2000).

[23] A. Beveratos, R. Brouri, T. Gacoin, J.-P. Poizat, and P. Grangier, *Nonclassical radiation from diamond nanocrystals*, Phys. Rev. A **64**, 061802 (2001).

[24] van der Sar, T, Z. H. Wang, M. S. Blok, H. Bernien, T. H. Taminiau, D. M. Toyli, D. A. Lidar, D. D. Awschalom, R. Hanson, and V. V. Dobrovitski, *Decoherence-protected quantum gates for a hybrid solid-state spin register*, Nature **484**, 82 (2012).

[25] L. Robledo, L. Childress, H. Bernien, B. Hensen, Alkemade, Paul F A, and R. Hanson, *High-fidelity projective read-out of a solid-state spin quantum register*, Nature **477**, 574 (2011).

[26] J. R. Maze, P. L. Stanwix, J. S. Hodges, S. Hong, J. M. Taylor, P. Cappellaro, L. Jiang, Dutt, M V Gurudev, E. Togan, A. S. Zibrov, A. Yacoby, R. L. Walsworth, and M. D. Lukin, *Nanoscale magnetic sensing with an individual electronic spin in diamond*, Nature **455**, 644 (2008).

[27] V. R. Horowitz, B. J. Alemán, D. J. Christle, A. N. Cleland, and D. D. Awschalom, *Electron spin resonance of nitrogen-vacancy centers in optically trapped nanodiamonds*, Proc. Natl. Acad. Sci. U.S.A. **109**, 13493 (2012).

[28] J. Tisler, G. Balasubramanian, B. Naydenov, R. Kolesov, B. Grotz, R. Reuter, J.-P. Boudou, P. A. Curmi, M. Sennour, A. Thorel, M. Börsch, K. Aulenbacher, R. Erdmann, P. R. Hemmer, F. Jelezko, and J. Wrachtrup, *Fluorescence and spin properties of defects in single digit nanodiamonds*, ACS Nano **3**, 1959 (2009).

[29] A. Faraon, C. Santori, Z. Huang, V. M. Acosta, and R. G. Beausoleil, *Coupling of nitrogen-vacancy centers to photonic crystal cavities in monocrystalline diamond*, Phys. Rev. Lett. **109**, 033604 (2012).

[30] C. Santori, P. E. Barclay, K.-M. C. Fu, R. G. Beausoleil, S. Spillane, and M. Fisch, *Nanophotonics for quantum optics using nitrogen-vacancy centers in diamond*, Nanotechnology **21**, 274008 (2010).

[31] T. M. Babinec, Hausmann, Birgit J M, M. Khan, Y. Zhang, J. R. Maze, P. R. Hemmer, and M. Loncar, *A diamond nanowire single-photon source*, Nat. Nanotechnol. **5**, 195 (2010).

[32] T. Schröder, F. Gädeke, M. J. Banholzer, and O. Benson, *Ultrabright and efficient single-photon generation based on nitrogen-vacancy centres in nanodiamonds on a solid immersion lens*, New J. Phys. **13**, 055017 (2011).

[33] K.-M. C. Fu, P. E. Barclay, C. Santori, A. Faraon, and R. G. Beausoleil, *Low-temperature tapered-fiber probing of diamond nitrogen-vacancy ensembles coupled to gap microcavities*,

New J. Phys. **13**, 055023 (2011).

[34] A. Faraon, P. E. Barclay, C. Santori, K.-M. C. Fu, and R. G. Beausoleil, *Resonant enhancement of the zero-phonon emission from a colour centre in a diamond cavity*, Nature Photon. **5**, 301 (2011).

[35] O. Benson, *Assembly of hybrid photonic architectures from nanophotonic constituents*, Nature **480**, 193 (2011).

[36] S. Schietinger, M. Barth, T. Aichele, and O. Benson, *Plasmon-enhanced single photon emission from a nanoassembled metal-diamond hybrid structure at room temperature*, Nano Lett. **9**, 1694 (2009).

[37] T. van der Sar, J. Hagemeier, W. Pfaff, E. C. Heeres, S. M. Thon, H. Kim, P. M. Petroff, T. H. Oosterkamp, D. Bouwmeester, and R. Hanson, *Deterministic nanoassembly of a coupled quantum emitter–photonic crystal cavity system*, Appl. Phys. Lett. **98**, 193103 (2011).

[38] R. Kolesov, B. Grotz, G. Balasubramanian, R. J. Stöhr, A. A. L. Nicolet, P. R. Hemmer, F. Jelezko, and J. Wrachtrup, *Wave–particle duality of single surface plasmon polaritons*, Nature Phys. **5**, 470 (2009).

[39] A. Huck, S. Kumar, A. Shakoor, and U. L. Andersen, *Controlled coupling of a single nitrogen-vacancy center to a silver nanowire*, Phys. Rev. Lett. **106**, 096801 (2011).

[40] Michaelis, Hettich, Mlynek, and Sandoghdar, *Optical microscopy using a single-molecule light source*, Nature **405**, 325 (2000).

[41] A. Cuche, A. Drezet, Y. Sonnefraud, O. Faklaris, F. Treussart, J.-F. Roch, and S. Huant, *Near-field optical microscopy with a nanodiamond-based single-photon tip*, Opt. Express **17**, 19969 (2009).

[42] A. Cuche, O. Mollet, A. Drezet, and S. Huant, *"deterministic" quantum plasmonics*, Nano Lett. **10**, 4566 (2010).

[43] M. Frimmer, Y. Chen, and A. F. Koenderink, *Scanning emitter lifetime imaging microscopy for spontaneous emission control*, Phys. Rev. Lett. **107**, 123602 (2011).

[44] J. Tisler, T. Oeckinghaus, R. J. Stoehr, R. Kolesov, R. Reuter, F. Reinhard, and J. Wrachtrup, *Single defect center scanning near-field optical microscopy on graphene*, Nano Lett. **13**, 3152 (2013).

[45] R. Beams, D. Smith, T. W. Johnson, S.-H. Oh, L. Novotny, and A. N. Vamivakas, *Nanoscale fluorescence lifetime imaging of an optical antenna with a single diamond NV center*, Nano Lett. **13**, 3807 (2013).

[46] A. W. Schell, P. Engel, J. F. M. Werra, C. Wolff, K. Busch, and O. Benson, *Scanning single quantum emitter fluorescence lifetime imaging: Quantitative analysis of the local density of photonic states*, Nano Lett. **14**, 2623 (2014).

[47] L. Rondin, J.-P. Tetienne, T. Hingant, J.-F. Roch, P. Maletinsky, and V. Jacques, *Magnetometry with nitrogen-vacancy defects in diamond*, Rep. Prog. Phys. **77**, 056503 (2014).

[48] C. L. Degen, *Scanning magnetic field microscope with a diamond single-spin sensor*, Appl. Phys. Lett. **92**, 243111 (2008).

[49] J. M. Taylor, P. Cappellaro, L. Childress, L. Jiang, D. Budker, P. R. Hemmer, A. Yacoby, R. Walsworth, and M. D. Lukin, *High-sensitivity diamond magnetometer with nanoscale resolution*, Nat. Phys. **4**, 810 (2008).

[50] G. Balasubramanian, I. Y. Chan, R. Kolesov, M. Al-Hmoud, J. Tisler, C. Shin, C. Kim, A. Wojcik, P. R. Hemmer, A. Krueger, T. Hanke, A. Leitenstorfer, R. Bratschitsch, F. Jelezko, and J. Wrachtrup, *Nanoscale imaging magnetometry with diamond spins under ambient conditions*, Nature **455**, 648 (2008).

[51] P. Maletinsky, S. Hong, M. S. Grinolds, B. Hausmann, M. D. Lukin, R. L. Walsworth, M. Loncar, and A. Yacoby, *A robust scanning diamond sensor for nanoscale imaging with single nitrogen-vacancy centres*, Nat. Nanotechnol. **7**, 320 (2012).

[52] C. Bradac, T. Gaebel, N. Naidoo, J. R. Rabeau, and A. S. Barnard, *Prediction and measurement of the size-dependent stability of fluorescence in diamond over the entire nanoscale*, Nano Lett. **9**, 3555 (2009).

[53] F. A. Inam, T. Gaebel, C. Bradac, L. Stewart, M. J. Withford, J. M. Dawes, J. R. Rabeau, and M. J. Steel, *Modification of spontaneous emission from nanodiamond colour centres on a structured surface*, New J. Phys. **13**, 073012 (2011).

[54] L. H. G. Tizei and M. Kociak, *Spectrally and spatially resolved cathodoluminescence of nanodiamonds: local variations of the NV^0 emission properties*, Nanotechnology **23**, 175702 (2012).

[55] P. V. Ruijgrok, R. Wüest, A. A. Rebane, A. Renn, and V. Sandoghdar, *Spontaneous emission of a nanoscopic emitter in a strongly scattering disordered medium*, Opt. Express **18**, 6360 (2010).

[56] H. Schniepp and V. Sandoghdar, *Spontaneous emission of europium ions embedded in dielectric nanospheres*, Phys. Rev. Lett. **89**, 257403 (2002).

[57] F. Jelezko and J. Wrachtrup, *Single defect centres in diamond: A review*, Phys. Stat. Sol. (a) **203**, 3207 (2006).

[58] S. Schietinger, *private communication*.

[59] C. Bradac, T. Gaebel, N. Naidoo, M. J. Sellars, J. Twamley, L. J. Brown, A. S. Barnard, T. Plakhotnik, A. V. Zvyagin, and J. R. Rabeau, *Observation and control of blinking nitrogen-vacancy centres in discrete nanodiamonds*, Nat. Nanotechnol. **5**, 345 (2010).

[60] S. Schietinger, T. Schröder, and O. Benson, *One-by-one coupling of single defect centers in nanodiamonds to high-q modes of an optical microresonator*, Nano Lett. **8**, 3911 (2008).

[61] R. Chapman and T. Plakhotnik, *Quantitative luminescence microscopy on nitrogen-vacancy centres in diamond: Saturation effects under pulsed excitation*, Chem. Phys. Lett. **507**, 190 (2011).

[62] Alegre, Thiago P. Mayer, C. Santori, G. Medeiros-Ribeiro, and R. G. Beausoleil, *Polarization-selective excitation of nitrogen vacancy centers in diamond*, Phys. Rev. B **76**, 165205 (2007).

[63] L. Robledo, H. Bernien, T. van der Sar, and R. Hanson, *Spin dynamics in the optical cycle of single nitrogen-vacancy centres in diamond*, New J. Phys. **13**, 025013 (2011).

[64] T. Plakhotnik, W. Moerner, V. Palm, and U. P. Wild, *Single molecule spectroscopy: maximum emission rate and saturation intensity*, Opt. Commun. **114**, 83 (1995).

[65] C.-T. Tai, *Dyadic Green functions in electromagnetic theory*, volume 272, IEEE press New York, 1994.

[66] H. Mertens, A. F. Koenderink, and A. Polman, *Plasmon-enhanced luminescence near noble-metal nanospheres: Comparison of exact theory and an improved Gersten and Nitzan model*, Phys. Rev. B **76**, 115123 (2007).

[67] H. Urbach and G. Rikken, *Spontaneous emission from a dielectric slab*, Phys. Rev. A **57**, 3913 (1998).

[68] A. F. Koenderink, M. Kafesaki, B. C. Buchler, and V. Sandoghdar, *Controlling the resonance of a photonic crystal microcavity by a near-field probe*, Phys. Rev. Lett. **95**, 153904 (2005).

[69] T. van der Sar, J. Hagemeier, W. Pfaff, E. Heeres, S. Thon, H. Kim, P. Petroff, O. Tjerk, D. Bouwmeester, and R. Hanson, *Effect of a nanoparticle on the optical properties of a photonic crystal cavity: theory and experiment*, J. Opt. Soc. Am. B **29**, 698 (2012).